FEA–CFD NUMERICAL APPROACHES IN THE DESIGN OF THE FAST PERIODIC SHUTTER FOR FAXTOR-BL31 AT ALBA

A. Cano Navarro*, A. Carballedo Costa, A. Patera, M. Quispe, B. de Abreu Francisco
ALBA Synchrotron, Cerdanyola del Vallès, Spain

Abstract

In the context of the experiments to be carried out at the fast X-ray tomography and radioscopy beamline (FAXTOR-BL31) of the ALBA synchrotron, a Fast Periodic Shutter (FPS) is being designed. Its purpose is to prevent a high dose rate on the sample and to provide synchronization with the acquisition protocol. This FPS is based on the combination of tungsten blades driven by a servomotor. This work details the FEA-CFD numerical simulations (ANSYS) developed for the FPS's thermo-mechanical design. Models considered steady-state and transient (periodic) conditions. Initial steady-state analysis (under vacuum) quantified baseline mechanical stress. Subsequently, a coupled CFD approach modeled the cooling gas and forced convection effects. The thermal modeling incorporated combined synchrotron radiation and Stefan-Boltzmann radiation modeling. The main objective of these simulations is to quantify the resulting thermo-mechanical stress and temperature distribution to ensure the structural integrity of the blades. Complementarily, the influence of air resistivity on rotor performance and the temperature dynamic considering air cooling and periodic radiation were examined.

BACKGROUND

FAXTOR (FAst X-ray TOmography and Radioscopy) is the first hard X-ray imaging beamline constructed at ALBA Synchrotron. It is a versatile beamline designed for quasi-real-time three-dimensional computed tomography. Beyond conventional 3D tomography, FAXTOR provides the user community with a powerful tool for investigating the dynamics of processes occurring at the micrometric scale by means of X-ray imaging [1].

As part of its projects, a Fast Periodic Shutter (FPS) is being designed, with the aim of preventing high dose rates on the sample and providing synchronization with the acquisition protocol. This work presents the results of FEA–CFD simulations of this design, carried out using ANSYS® [2].

GEOMETRICAL MODEL

The FPS consists of a titanium rotor integrating four TRIAMET tubes ($\phi_{ext} = 18\,mm$, $L = 60\,mm$) through which the beam passes. The rotor is supported by lateral aluminium mounts, which are themselves fixed to a granite base (Fig. 1). All components are housed within an aluminium enclosure. Table 1 summarizes the main FPS material properties: Poisson ratio ν, thermal conductivity λ, Young's modulus E, emissivity ε, density ρ, and specific heat capacity C_p [3].

* adrian.cano.nav@gmail.com

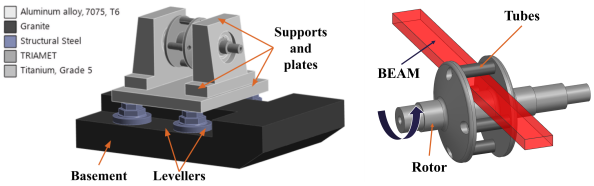

(a) Full assembly geometry (b) Reduced geometry

Figure 1: Parts & materials of the FPS system.

Table 1: Properties of FPS Materials

Material	ν [-]	λ [W/mK]	E [MPa]	ε [-]	ρ [kg/m^3]	C_p [J/kgK]
TRIAMET	0.27	96	3.1×10^5	0.45	17 000	150
Ti Gr. 5	0.34	7.00	1.05×10^5	0.40	4470	580

SIMULATION SETUP

Simulation Cases

Table 2 presents the cases simulated in this work. M1 and M2 are static structural vacuum simulations, while M3 is a mechanical computational fluid dynamics (CFD) case. MS1, SS1, SS2 and SS3 are steady-state thermal simulations, whereas TR1 is a FEM transient thermal case and TR2 is its lumped-parameter counterpart implemented in Simulink [4]. Finally, TM-CFD1 is the thermal CFD study.

Table 2: Simulation Cases Summary

Type	Codes	Geometry
Mechanical	M1, M2 & M3	Reduced
Map simplification	MS1	Prism benchmark
Steady-state thermal	SS1, SS2 & SS3	Full assembly
Transient thermal	TR1 & TR2	Reduced & lumped model
Thermal CFD	TM-CFD1	Full assembly

Mesh Generation

Unstructured meshes were used, with refinement concentrated in the tubes, where thermal gradients are highest (Fig. 2). A mesh convergence study was performed for all cases, ensuring that variations in the output variables remained below <5%.

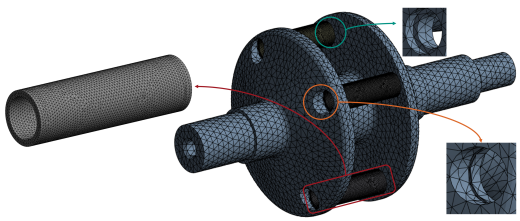

Figure 2: Example of refined mesh near beam footprint.

Boundary Conditions

Mechanical Simulations Rotational speeds (ω_{rot}) of up to 15 000 rpm were considered, with centrifugal loads implemented as body forces. Contact interactions were modelled as either bonded (M1) or frictional (M2; $\mu = 0.2$). In case M3, aerodynamic loads obtained from CFD simulations were additionally included to assess the effects of airflow.

Thermal Simulations A total heat input of 300 W (peak of 1.1 W mm^{-2}) was applied to the tubes from Synrad® bending magnet (BM) and insertion device (ID) power maps. Table 3 lists the input parameters, where E_b is the beam energy, I_d is the design current, M_s is the magnetic source, and ρ_c is the bending radius of curvature [5].

For efficiency, power was applied to a single tube, assuming periodic thermal symmetry unless otherwise stated.

Table 3: BM and ID Input Parameters for ALBA II

Source	E_b [GeV]	I_d [mA]	M_s [T]	ρ_c [m]
BM	3	400	1.42	7.047
ID	3	400	Multipole Wiggler [1]	–

A parametric steady-state analysis defined the thermal operating envelope. In SS1, T_{amb} was set to 23, 50 and 80 °C, while h_{ext} was set to 100, 150 and 200 W m^{-2} K^{-1}. SS2 included internal convection, and SS3 added radiation through prescribed emissivities (Table 2). In TR1, radiation was neglected and ω_{rot} ranged from 150 rpm to 1500 rpm.

Thermal CFD TM-CFD1 modelled rotor-induced forced convection at 15 000 rpm using a turbulent k-ω SST model. The thermal load was applied to one rotating tube and solved at steady state with SIMPLEC, second-order schemes and gravity included.

RESULTS AND DISCUSSION

Mechanical

Mesh convergence results for cases M1–M3 are presented in Fig. 3, showing their evolution with mesh refinement.

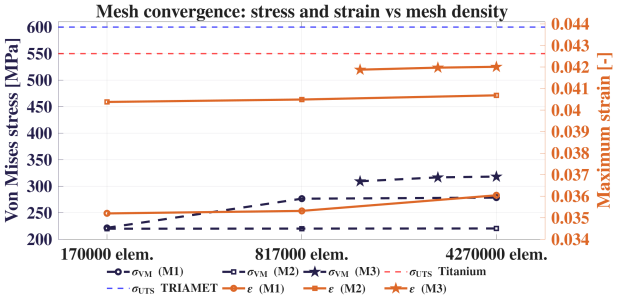

Figure 3: Max. von Mises stress & strain for M1, M2 & M3.

Stress levels σ_{VM} (purple) remain well below the ultimate tensile strength σ_{UTS} of both materials (red and blue dash lines), ensuring safe operation thanks to a minimum safety factor of 1.5. Meanwhile, strain ε (orange) reports negligible sensitivity to mesh refinement.

Thermal

Map Simplification To validate the reduction strategy (MS1, Table 2), the Synrad® power map, defined as $\{(x_i, y_j, q_{ij})\}$ with q_{ij} the local power density (PD), was simplified in MATLAB® to reduce CPU cost while preserving the thermal footprint [6].

The workflow, summarized in Fig. 4, consists of: (i) symmetrization of the map, (ii) identification of high-gradient regions, (iii) adaptive spatial partitioning, (iv) block-wise averaging, & (v) clustering into a reduced number of levels followed by rescaling to ensure total power conservation.

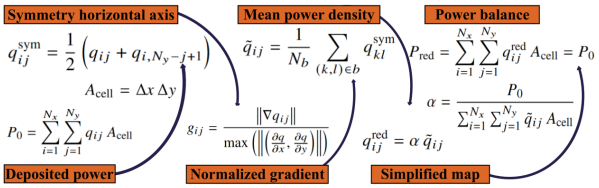

Figure 4: Workflow procedure to simplify the Synrad® map.

The number of PD levels was progressively reduced until the deviation in peak temperature between the original & simplified maps remained <5%.

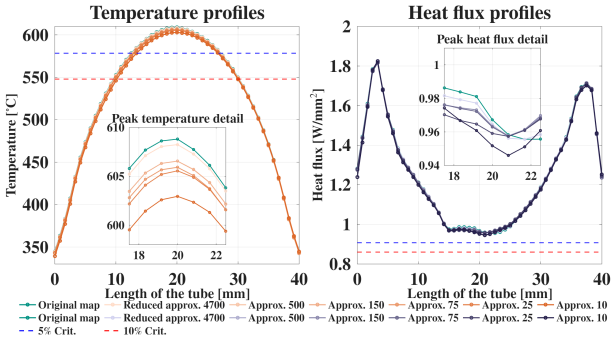

Figure 5: Temperature and heat flux profiles for MS1.

As shown in Fig. 5, temperature and heat-flux profiles are preserved across reduction levels, with peak values and beam-footprint gradients differing by less than 5%. The spatial comparison in Fig. 6 confirms that the simplified map retains the location and extent of the high-intensity region while coarsening low-gradient areas.

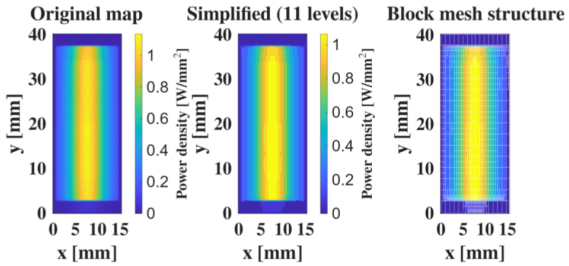

Figure 6: PD distribution comparison between both maps.

Thus, the proposed reduction significantly decreases CPU cost while maintaining physical fidelity of the thermal load.

Steady-State Thermal As presented in Fig. 7, T_{max} varies nearly linearly, increasing with T_{amb} and decreasing with h, with differences of ~150 °C between extreme cases.

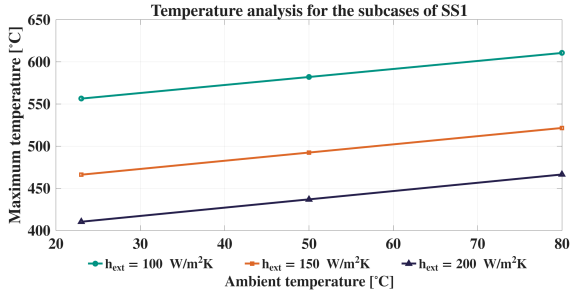

Figure 7: Max. system temperature f(T_{amb}, h_{ext}) for SS1.

The worst case (T_{amb} = 80 °C, h = 100 W m^{-2} K^{-1}) reaches 610.57 °C. The corresponding temperature distribution (Fig. 8a) reveals highly localized heating at the beam footprint and limited conduction through the structure.

A representative operating condition (T_{amb} = 50 °C, h = 200 W m^{-2} K^{-1}) was selected, yielding 436.94 °C. Fig. 8b compares this case of SS1 with SS2 & SS3. Internal convection has negligible impact (<0.1 °C), whereas radiation reduces the peak temperature to 431.72 °C.

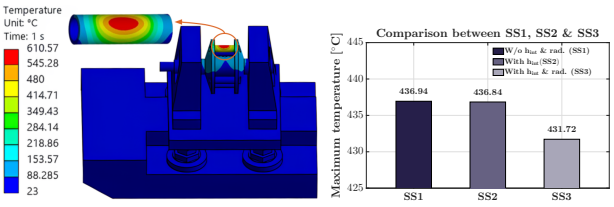

(a) Temperature for the worst case. (b) T_{max} for SS1-SS3.

Figure 8: Temperature results for SS1, SS2 & SS3.

Hence, Fig. 8 shows convection & radiation dominance, with conduction acting as a secondary mechanism.

Transient Thermal On TR1, the transient heat load was applied by periodically shifting the simplified map over the tube surface, assuming $\frac{1}{4}$ revolution per step. This reproduces the rotor-beam relative motion while keeping the transient FEM cost manageable.

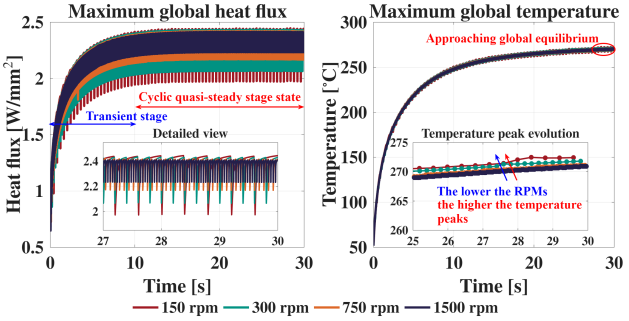

Figure 9: Transient FEM stability analysis (TR1).

As shown in Fig. 9, the system reaches a periodic steady-state, with oscillations around a mean temperature that increases with rotational speed. Agreement with steady-state predictions without radiation validates the transient formulation. To extend the analysis beyond FEM limits, a lumped-parameter (LP) model was developed (TR2, Fig. 10) [7].

For validation purposes, TR1 & TR2 were compared at 1500 rpm at 30 s of simulated time (Table 4).

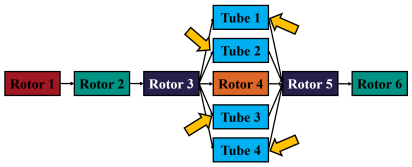

Figure 10: Scheme of the LP model.

Table 4: Thermal Comparison Between TR1 and TR2

Component	$T_{\text{max}}^{\text{TR1}}$ [°C]	$T_{\text{max}}^{\text{TR2}}$ [°C]	$T_{\text{average}}^{\text{TR1}}$ [°C]	$T_{\text{average}}^{\text{TR2}}$ [°C]
Tube 1	271.05	239.6	188.08	183.25

Once validated, the LP was used to simulate at 15 000 rpm and power applied to one tube and four tubes. These results (Table 5) confirm higher rotor & bar temperatures than in the single-tube case, due to cumulative multi-tube irradiation.

Table 5: TR2 Temperature After 1000 Simulated Seconds

Component	Tube 1	Rotor 2	Rotor 3	Rotor 4
T_{average} with 1 tube [°C]	210.7	51.15	57.92	56.84
T_{max} with 1 tube [°C]	241.2	74.63	112.6	70.12
T_{average} with 4 tubes [°C]	221.3	54.59	81.65	63.29
T_{max} with 4 tubes [°C]	251.7	77.64	117.25	77.23

Thermal CFD Model

Figure 11 shows the rotor thermal field and chamber velocity vectors. The maximum temperature was 186.63 °C, located in the heat deposition region.

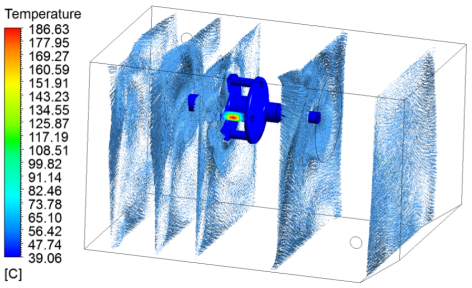

Figure 11: Temperature & velocity field for case TM-CFD1.

Rotor-induced recirculation enhances convective cooling, leading to a lower peak temperature than that predicted with experimental heat-transfer coefficients and confirming the conservative nature of the latter approach.

CONCLUSIONS & FUTURE WORK

Therefore, key findings are summarized as follows:

1. Safe mechanical operation verified up to 15 000 rpm thanks to M1, M2 & M3.
2. Convection dominates the thermal response, with radiation secondary, while reduced maps and TR1-TR2 models preserve accuracy under extreme conditions.
3. Future work will address full CFD validation and experimental correlation.

REFERENCES

[1] A. Patera *et al.*, "FaXToR: the hard X-ray micro-tomography beamline at the Spanish synchrotron ALBA," *J. Synchrotron Radiat.*, vol. 33, pp. 207–217, 2026, doi:10.1107/S160057752500997X.

[2] Ansys website, www.ansys.com/

[3] MatWeb Material Property Data website, www.matweb.com/

[4] MathWorks Simulink website, es.mathworks.com/products/simulink.html

[5] CERN MolFlow/Synrad documentation, molflow.docs.cern.ch/

[6] MATLAB website, www.mathworks.com/products/matlab.html

[7] L. M. Volpe *et al.*, "Thermal model validation for the cryogenic mirror systems for Sirius/LNLS," in *Proc. MEDSI'20*, Chicago, IL, USA, Jul. 2021, pp. 320–323, doi:10.18429/JACoW-MEDSI2020-WEPC07.